A Bayesian approach for condition assessment and damage alarm of bridge expansion joints using long-term structural health monitoring data

Y.Q. Ni*, Y.W. Wang, C. Zhang

Department of Civil and Environmental Engineering, The Hong Kong Polytechnic University, Hung Hom, Kowloon, Hong Kong

ABSTRACT

Premature failure of bridge expansion joints has been increasingly observed in recent years, and nowadays it becomes a major concern of bridge owners. A better understanding of their performance in service is highly desired. Deterministic linear regression models between bridge temperature and expansion joint displacement have widely been adopted to characterize the in-service performance of bridge expansion joints. When such a regression pattern is elicited using real-time monitoring data, the deterministic models fail to account for uncertainty inherent in the monitoring data and interpret the model error. In this study, a probabilistic approach for characterization of the regression pattern between bridge temperature and expansion joint displacement by use of Structural Health Monitoring (SHM) data and for SHM-based condition assessment and damage alarm of bridge expansion joints is developed in the Bayesian context. The proposed approach enables to account for the uncertainty contained in the monitoring data and quantify the model error and the prediction uncertainty. By combining the Bayesian regression model and reliability theory, an anomaly index is formulated to evaluate the health condition of the expansion joint when newly collected monitoring data are available and to provide damage alarm once the probability of damage exceeds a certain threshold. In the case study, real-world monitoring data acquired from a cable-stayed bridge are used to illustrate the proposed approach, including examining the appropriateness of the design values of expansion joint displacements under extreme temperatures in serviceability limit state.

1. Introduction

Expansion joints are important components in bridge structures, which are designed to accommodate the relative movement between bridge deck and abutments, ensuring the serviceability of bridges [1]. Due to the direct and repetitive impact of vehicle loads, expansion joints often become the weakest part of bridges, especially for long-span bridges where premature failures of the expansion joints have been increasingly observed, resulting in considerable repair and maintenance costs [2–4]. Several surveys have indicated that the service life of expansion joints is frequently much lower than expected. For instance, the Akashi-Kaikyo Bridge, the world's longest suspension bridge with a main span of 1991 m, experienced fatigue cracks in the connection pin of the expansion joints only three years after the bridge was opened to traffic [5]. The suspension Runyang Bridge with a main span of 1490 m suffered the need for the expansion joints to be repaired after three-year service [6]. The suspension Jiangyin Bridge with a main span of 1385 m suffered excessive wear and transversal shear failure of bearings in expansion joints after only four years since operation [4]. The

expansion joints in the Martinus Nijhoff Bridge have been repaired several times in recent years [7].

Apparently, an understanding of the real performance of bridge expansion joints during in-service operation is highly desired in regard to their safety and maintenance. Traditional manual inspection methods are typically expensive, inefficient, and incapable of offering a timely alarm on possible deterioration or malfunctioning of expansion joints. In contrast, Structural Health Monitoring (SHM) technology provides a sensor-based quantitative and objective means to continuously gain authentic information about the in-situ performance of expansion joints, which enables potential failure to be foreseen at an early stage. Research efforts have been made towards this direction. Ni et al. [8] proposed a procedure for design verification and condition assessment of expansion joints using the long-term monitoring data. A normal temperature-displacement pattern was established through linear regression analysis, with which the maximum displacement range and cumulative movement were evaluated. Ding and Li [9] investigated the effects of temperature, traffic and wind on the displacement of expansion joints. After removing the effect of

---

environmental conditions on expansion joint displacement, potential damage in expansion joints was detected by using statistical process control. Making use of SHM monitoring data, Guo et al. [4] analyzed the expansion joint displacement of a long-span steel bridge equipped with viscous dampers, with an emphasis on the influence of the dampers on the displacement. Sun and Zhang [6] clarified the failure mechanism of the expansion joints in a suspension bridge through both field tests and numerical study, and finally put forward suggestions to improve expansion joint performance. Huang et al. [10] proposed the use of representative temperature to establish the Displacement-Temperature Relationship (DTR) model for expansion joints. By constructing a mean value control chart for the error of the baseline model, a performance-alarm approach was proposed for the assessment of expansion joints.

While confirming a linearly proportional relationship, all the previous studies adopted deterministic (linear) regression models to characterize the DTR for bridge expansion joints. However, uncertainties inevitably exist in the monitoring data due to environmental variability and measurement noise. The deterministic models fail to account for the uncertainties inherent in the monitoring data and to interpret the model error, and as a result they might not reflect the authentic performance of expansion joints and lead to inaccurate diagnostic and prognostic results in the presence of various uncertainties. In this regard, probabilistic regression models are preferable in characterizing the DTR of expansion joints and evaluating the probability of potential damage. Being a powerful analytic tool as regards quantifying uncertainty, Bayesian inference has been growingly applied for model updating, system identification and damage detection [11–22]. To the best of the authors' knowledge, however, no investigation has been devoted to addressing the condition assessment and damage detection of bridge expansion joints in the context of Bayesian inference.

In this study, a novel approach which enables probabilistic condition assessment and damage alarm of bridge expansion joints will be developed in the context of Bayesian inference. Making use of long-term SHM data, a Bayesian (linear) regression model is first formulated to characterize the correlation pattern between the thermal movement of expansion joints and the effective temperature of bridge deck. Different from the traditional deterministic regression models, the formulated model explicitly interprets uncertainties arising from measurement and model errors and enables to quantify prediction uncertainty when newly collected data are presented. By combining the Bayesian regression model and reliability theory, an anomaly index is formulated to quantitatively evaluate the probability of failure of expansion joints. More importantly, the anomaly index can be evolutionarily evaluated and refined along with successively collected monitoring data, enabling to foresee the possible failure of expansion joints at an early stage. The ability of this fully date-driven method for prediction, uncertainty qualification, condition assessment and damage alarm of bridge expansion joints will be verified by using real-world monitoring data from a cable-stayed bridge.

This paper is organized as follows. Section 1 briefly reviews the problem and reports on premature failure of bridge expansion joints, and the state-of-the-art research on evaluating the performance of bridge expansion joints in service. In Section 2, the Bayesian DTR model characterizing the normal pattern of bridge expansion joints is formulated, and an anomaly index quantitatively evaluating the probability of failure is developed. In Section 3, the proposed method for probabilistic condition assessment and damage alarm of bridge expansion joints is verified with the use of real-world monitoring data acquired from a long-span cable-stayed bridge. Conclusions are drawn in Section 4.

2. Formulation of Bayesian DTR model and anomaly index

As stated above, the longitudinal displacement of bridge expansion joints is primarily induced by temperature fluctuations. Of interest is an

obvious linear relationship between displacement and temperature which is the normal pattern of bridge expansion joints. To formulate the DTR model, multi-channel temperature monitoring data are usually required to characterize the bridge temperature field. In this study, the effective temperature of bridge deck cross-section is employed to account for the correlation between bridge expansion joint displacement and temperature variation. Making use of the formulated Bayesian DTR model and reliability theory, an anomaly index is elicited for condition assessment and damage alarm of bridge expansion joints.

2.1. Extraction of effective temperature

For a long-span bridge equipped with an SHM system, there is often a dense array of temperature sensors deployed at various locations of the bridge to monitor the temperature variation at different structural portions. As a result, a considerable amount of temperature data from different measurement points are available, and some of them might be highly correlated. In practice, only certain representative temperatures extracted from massive monitoring data are necessary to formulate the DTR model. There are three typical representative temperatures which are commonly used in practice, i.e., mean temperature, effective temperature, and principal components of temperature [10,23]. The mean temperature, a simple version of the representative temperature, represents an average of all measured temperatures; while the principal components of temperatures are computed by the Principal Component Analysis (PCA) to reflect the major temperature fluctuations. Both the mean temperature and principal components of temperature don't have an explicit relationship with the thermal movement of expansion joints. In principle, temperature distribution over a bridge deck cross-section can be divided into two parts: the effective temperature that contributes to the bridge longitudinal movements and the differential temperature that contributes to the bridge bending deformations. In this regard, the effective temperature, which accounts for thermal movements along the bridge longitudinal direction, is a physically interpretative quantity in explicit relation to the displacement of expansion joints [23]. According to the definition, the effective temperature of a cross-section can be expressed as

$$T = \frac{1}{A} \iint_A \bar{T}(x, y) dx dy \tag{1}$$

where A=area of the cross-section; and $\bar{T}(x, y)$=two-dimensional temperature over the cross-section. With the monitoring data from temperature sensors located at a number of discrete locations, it is difficult to calculate the effective temperature directly by Eq. (1). In practice, the effective temperature can be estimated using the monitoring data acquired from a bridge deck cross-section with the most temperature sensors deployed, by

$$T = \sum_{i=1}^{k} \frac{A_i}{A} \bar{T}_i \tag{2}$$

where $A_i = i$th subarea; A=the gross area of the cross-section; $\bar{T}_i$=measured temperature at the ith subarea; and k=number of subareas divided for the cross-section. The above approximation assumes that the temperature at each subarea is identical, and the effective temperature is obtained by a weighted average of temperatures measured from all subareas (the material properties in subareas might be different, e.g., steel, concrete, asphalt).

2.2. Bayesian modelling

Bayesian regression differs from traditional regression in that the model parameters are treated more as random variables than fixed constants. As the model parameters are random variables, more information can be incorporated into the model by construction of a probability distribution that describes the uncertainty involved in the

model parameters. In addition, it gives rise to the (posterior) distribution of the prediction, which greatly facilitates the reliability-based assessment of structural condition.

Suppose we have n sets of independent observations $\{(y_\alpha, x_\alpha); \quad \alpha = 1, 2, \cdots, n\}$, where y_α's are random response variables (e.g., displacement of expansion joints) and x_α's are vectors of k-dimensional explanatory variables (e.g., effective temperatures). The linear regression model of the relationship between the response variables and the explanatory variables can be generally written as

$$y_\alpha = \beta_1 x_{\alpha 1} + \beta_2 x_{\alpha 2} + \cdots + \beta_k x_{\alpha k} + \varepsilon_\alpha, \quad \alpha = 1, \cdots, n \tag{3}$$

where the errors ε_α's are independently, normally distributed random variables with mean zero and variance σ^2. Eq. (3) can be expressed compactly in matrix form as

$$y = X\beta + \varepsilon, \quad \varepsilon \sim N(0, \sigma^2 I) \tag{4}$$

where

$$y = \begin{bmatrix} y_1 \\ y_2 \\ \vdots \\ y_n \end{bmatrix}, \quad \beta = \begin{bmatrix} \beta_1 \\ \beta_2 \\ \vdots \\ \beta_k \end{bmatrix}, \quad X = \begin{bmatrix} x_{11} & x_{12} & \cdots & x_{1k} \\ x_{21} & x_{22} & \cdots & x_{2k} \\ \vdots & \vdots & \ddots & \vdots \\ x_{n1} & x_{n2} & \cdots & x_{nk} \end{bmatrix}, \quad \varepsilon = \begin{bmatrix} \varepsilon_1 \\ \varepsilon_2 \\ \vdots \\ \varepsilon_n \end{bmatrix}$$

and I represents the unit matrix of dimension n. It is common to set the first column of X to a constant value of 1 so that β_1 is an intercept term. Using the definition of multivariate normal distribution, the likelihood function can be written as

$$f(y|X, \beta, \sigma^2) = \frac{1}{(2\pi\sigma^2)^{n/2}} \exp\left[-\frac{(y - X\beta)^T(y - X\beta)}{2\sigma^2}\right] \tag{5}$$

In Eq. (5), the likelihood function is expressed as the joint probability density function for all data conditional on the unknown parameters β and σ^2. To facilitate the Bayesian inference of the regression model, it is commonly assumed that (β, σ^2) has the Normal Inverted-Gamma prior which is the natural conjugate prior for linear regression [24–26]

$$f(\beta, \sigma^2) = f(\beta|\sigma^2)f(\sigma^2) \tag{6}$$

with

$$f(\beta|\sigma^2) = N\left(\beta_0, \sigma^2 \sum{}_0\right)$$
$$= \frac{1}{(2\pi\sigma^2)^{k/2} \cdot |\sum_0|^{1/2}} \exp\left[-\frac{(\beta - \beta_0)^T \sum_0^{-1}(\beta - \beta_0)}{2\sigma^2}\right]$$

$$f(\sigma^2) = IG\left(\frac{a}{2}, \frac{b}{2}\right) = \frac{\left(\frac{b}{2}\right)^{a/2}}{\Gamma\left(\frac{a}{2}\right)}(\sigma^2)^{-a/2-1}\exp\left(-\frac{b}{2\sigma^2}\right)$$

where $\sum_0$ is a symmetric positive definite matrix of size $k \times k$.

According to the Bayes' theorem, the posterior distribution $f(\beta, \sigma^2|y, X)$ is proportional to the likelihood function $f(y|X, \beta, \sigma^2)$ multiplied by the prior distribution $f(\beta, \sigma^2)$

$$f(\beta, \sigma^2|y, X) = f(y|X, \beta, \sigma^2) \times f(\beta, \sigma^2)$$
$$\propto (\sigma^2)^{-n/2}\exp\left[-\frac{(y - X\beta)^T(y - X\beta)}{2\sigma^2}\right] \times (\sigma^2)^{-k/2}\exp\left[$$
$$-\frac{(\beta - \beta_0)^T \sum_0^{-1}(\beta - \beta_0)}{2\sigma^2}\right]$$
$$\times (\sigma^2)^{-a/2-1}\exp\left(-\frac{b}{2\sigma^2}\right) \tag{7}$$

Combining the density functions and the joint posterior yields

$$f(\beta, \sigma^2|y, X) \propto (\sigma^2)^{-k/2}\exp\left\{-\frac{1}{2\sigma^2}(\beta^T[X^TX + \sum{}_0^{-1}]\beta \right.$$
$$\left. - 2\beta^T[X^Ty + \sum{}_0^{-1}\beta_0] + y^Ty + \beta_0^T \sum{}_0^{-1}\beta_0)\right\}$$
$$\times (\sigma^2)^{-(a+n)/2-1}\exp\left(-\frac{b}{2\sigma^2}\right) \tag{8}$$

After some manipulations, Eq. (8) can be further expressed as

$$f(\beta, \sigma^2|y, X) \propto (\sigma^2)^{-k/2}\exp\left\{-\frac{(\beta - \beta^*)^T(\sum^*)^{-1}(\beta - \beta^*)}{2\sigma^2}\right\}$$
$$\times (\sigma^2)^{-a^*/2-1}\exp\left(-\frac{b^*}{2\sigma^2}\right) \tag{9}$$

where

$$\sum{}^* = (X^TX + \sum{}_0^{-1})^{-1}$$
$$\beta^* = (X^TX + \sum{}_0^{-1})^{-1}(X^Ty + \sum{}_0^{-1}\beta_0)$$
$$a^* = a + n$$
$$b^* = b + y^Ty + \beta_0^T \sum{}_0^{-1}\beta_0 - (\beta^*)^T(\sum{}^*)^{-1}\beta^*$$

Note that Eq. (9) is again the kernel Normal Inverted-Gamma distribution. It can be factored as the conditional posterior distribution β multiplied by the marginal posterior distribution of σ^2

$$f(\beta, \sigma^2|y, X) = f(\beta|\sigma^2, y, X) \times f(\sigma^2|y) \tag{10}$$

where

$$\beta|\sigma^2, y, X \sim N\left(\beta^*, \sigma^2 \sum{}^*\right)$$

$$\sigma^2|y \sim IG\left(\frac{a^*}{2}, \frac{b^*}{2}\right)$$

Since the posterior distribution of the unknown parameters has been analytically elicited, we can easily delineate the characteristics of the posterior distribution, such as posterior mean, posterior median, posterior credible intervals and so on.

For the unknown model parameters β, their marginal posterior distribution can be obtained by integrating the variance parameter σ^2 out of the joint posterior, that is

$$f(\beta|y, X) = \int_0^\infty f(\beta, \sigma^2|y, X)d\sigma^2$$
$$\propto \int_0^\infty (\sigma^2)^{-(k+a^*)/2-1}\exp\left\{-\frac{(\beta - \beta^*)^T(\sum^*)^{-1}(\beta - \beta^*) + b^*}{2\sigma^2}\right\}d\sigma^2$$
$$= \int_0^\infty (\sigma^2)^{-(k+a^*)/2-1}\exp\left\{-\frac{B}{2\sigma^2}\right\}d\sigma^2 \tag{11}$$

where $B = (\beta - \beta^*)^T(\sum^*)^{-1}(\beta - \beta^*) + b^*$. Let $u = \frac{B}{2\sigma^2}$, then $\sigma^2 = \frac{B}{2u}$ and $\frac{d\sigma^2}{du} = -\frac{B}{2}u^{-2}$. By doing so, the marginal posterior distribution of β becomes

$$f(\beta|y, X) \propto \int_0^\infty \left(\frac{B}{2u}\right)^{-(k+a^*)/2-1}\exp\{-u\} \cdot \left(-\frac{B}{2}u^{-2}\right)du$$
$$= \left(\frac{B}{2}\right)^{-(k+a^*)/2}\int_0^\infty u^{(k+a^*)/2-1}\exp\{-u\}du \tag{12}$$

where the density function of u is Gamma function $f(u) = \frac{1}{\Gamma(\alpha)}u^{\alpha-1}\lambda^\alpha\exp(-\lambda u)$. When $\lambda = 1$, $\alpha = (k + a^*)/2$, then $f(u) = \frac{1}{\Gamma((k+a^*)/2)}u^{(k+a^*)/2-1}\exp(-u)$. From the properties of Gamma distribution, it follows that $\int_0^\infty u^{(k+a^*)/2-1}\exp\{-u\}du = \Gamma((k + a^*)/2)$. Thus, Eq. (12) can be expressed as

$$f(\beta|y, X) \propto \left(\frac{B}{2}\right)^{-(k+a^*)/2}\Gamma((k + a^*)/2) \propto B^{-(k+a^*)/2}$$
$$= [(\beta - \beta^*)^T(\sum{}^*)^{-1}(\beta - \beta^*) + b^*]^{-(k+a^*)/2}$$
$$= [1 + (\beta - \beta^*)^T(b^* \sum{}^*)^{-1}(\beta - \beta^*)]^{-(k+a^*)/2}$$
$$= \left[1 + \frac{1}{a^*}(\beta - \beta^*)^T\left(\frac{b^*}{a^*}\sum{}^*\right)^{-1}(\beta - \beta^*)\right]^{-(k+a^*)/2} \tag{13}$$

which is the kernel for the density of a multivariate Student-t distribution [25,27]. Thus, the marginal posterior distribution of $\boldsymbol{\beta}$ is Student-t distribution with

Mean: $\boldsymbol{\beta}^*$ Covariance: $\dfrac{b^*}{a^* - 2} \sum{}^*$

Given new measurements $\widehat{\boldsymbol{X}}$, the prediction distribution for the future observation $\widehat{\boldsymbol{y}}$ satisfies

$$\widehat{\boldsymbol{y}} = \widehat{\boldsymbol{X}}\boldsymbol{\beta} + \widehat{\boldsymbol{\varepsilon}} \tag{14}$$

which can be represented as $f(\widehat{\boldsymbol{y}}|\widehat{\boldsymbol{X}}, \boldsymbol{\beta}, \sigma^2)$. By integrating it with respect to the parameters $\boldsymbol{\beta}$ and σ^2, the posterior predictive distribution for the future observation $\widehat{\boldsymbol{y}}$ turns out to be the following multivariate Student-t distribution [28,29]

$$f(\widehat{\boldsymbol{y}}|\widehat{\boldsymbol{X}}) = \int f(\widehat{\boldsymbol{y}}|\widehat{\boldsymbol{X}}, \boldsymbol{\beta}, \sigma^2) f(\boldsymbol{\beta}, \sigma^2|\boldsymbol{y}, \boldsymbol{X}) d\boldsymbol{\beta} d\sigma^2$$

$$= \frac{\Gamma\left(\frac{a^*+q}{2}\right)}{\Gamma\left(\frac{a^*}{2}\right)(\pi a^*)^{q/2}} \left|\widehat{\sum}\right|^{-1/2} \left\{1 + \frac{1}{a^*}(\widehat{\boldsymbol{y}} - \widehat{\boldsymbol{\mu}})^T \widehat{\sum}{}^{-1} (\widehat{\boldsymbol{y}} - \widehat{\boldsymbol{\mu}})\right\}^{-(a^*+q)/2} \tag{15}$$

where $\widehat{\boldsymbol{\mu}} = \widehat{\boldsymbol{X}}\boldsymbol{\beta}^*$, and $\widehat{\sum} = \dfrac{b^*}{a^*}(I + \widehat{\boldsymbol{X}} \sum{}^{*-1} \widehat{\boldsymbol{X}}^T)$.

2.3. Gibbs sampler for Bayesian inference

With the assumption of natural conjugate prior, analytical expressions of joint posterior and marginal posterior distribution for the unknown parameters have been elicited in the previous section. However, when more general prior distributions and complex models with a larger set of unknown parameters are concerned, analytical solutions become impossible or computationally intractable. In such circumstances, Markov chain Monte Carlo (MCMC) algorithms offer a promising means regardless of prior distributions or complexity of the model. Gibbs sampler, one of MCMC algorithms, has been extensively used since its advent in the late 1990s [30]. As a special case of the more general Metropolis-Hasting algorithm, Gibbs sampler is preferable when sampling from a multivariate posterior is not feasible, but rather sampling from the conditional distributions for each variable is feasible [31]. The idea behind Gibbs sampler is to generate a sample from the distribution of each variable in turn, conditional on the current values of other variables. It is shown that the sample sequences constitute a Markov chain, and the stationary distribution of this Markov chain is just the sought-after posterior distribution of the variable. The iterative process of Gibbs sampler for generating the samples of $\boldsymbol{\beta}$ and σ^2 are as follows:

---

(1) Initialize the parameters $\{\boldsymbol{\beta}^{(0)}, \sigma^{2(0)}\}$ and let $k = 1$;
(2) Sample $\boldsymbol{\beta}^{(k)}$ from the conditional distribution $f(\boldsymbol{\beta}|\boldsymbol{y}, \boldsymbol{X}, \sigma^{2(k-1)})$;
(3) Sample $\sigma^{2(k)}$ from the conditional distribution $f(\sigma^2|\boldsymbol{y}, \boldsymbol{X}, \boldsymbol{\beta}^{(k)})$;
(4) Let $k = k + 1$, go back to (2) and (3) and repeat until L samples $\{\boldsymbol{\beta}^{(k)}, \sigma^{2(k)}: k = 1, \cdots, L\}$ are obtained.

As the number of Gibbs iterations increases to infinity, the draws from the conditional distributions converge to the joint posterior distribution $f(\boldsymbol{\beta}, \sigma^2|\boldsymbol{y}, \boldsymbol{X})$. In practice, after a large number of iterations, the marginal distributions of $\boldsymbol{\beta}$ and σ^2 can be approximated by the empirical distributions of samplers. More specifically, one repeats the Gibbs iterations L times (large enough for convergence) and saves the last H samplers of $\boldsymbol{\beta}^{(k)}$ and $\sigma^{2(k)}$ ($k = L - H, \cdots, L$) to estimate the marginal distributions of $\boldsymbol{\beta}$ and σ^2. Similarly, the posterior means, the standard errors and the 95% confidence intervals of $\boldsymbol{\beta}$ and σ^2 can be calculated by using the last H samplers. The 95% confidence interval is estimated by using 2.5% and 97.5% of the posterior samples. Note that the convergence of iteration must be judged before using the samples obtained

from Gibbs sampler to make inference, because it directly affects the accuracy of the statistical results. A concept of burn-in period (refers to L-H) is introduced to confirm the time period required for the draws to reach their stationary state. In practice, both visual inspection and Raftery-Lewis diagnostic [32,33] can be adopted to determine the length of the burn-in period.

With the posterior samples $\{\boldsymbol{\beta}^{(k)}, \sigma^{2(k)}: k = H, \cdots, L\}$, the predictive density of future value $\widehat{\boldsymbol{y}}$ given $\widehat{\boldsymbol{X}}$, can be approximated as [25]

$$f(\widehat{\boldsymbol{y}}|\widehat{\boldsymbol{X}}) = \int f(\widehat{\boldsymbol{y}}|\widehat{\boldsymbol{X}}, \boldsymbol{\beta}, \sigma^2) f(\boldsymbol{\beta}, \sigma^2|\boldsymbol{y}, \boldsymbol{X}) d\boldsymbol{\beta} d\sigma^2$$

$$\approx \frac{1}{L - H} \sum_{k=H}^{L} f(\widehat{\boldsymbol{y}}|\widehat{\boldsymbol{X}}, \boldsymbol{\beta}^{(k)}, \sigma^{2(k)}) \tag{16}$$

2.4. Damage alarming using anomaly index

The Bayesian regression model formulated above, which characterizes the correlation between expansion joint displacement and effective temperature, contains the uncertain parameters $\boldsymbol{\beta}$ and σ^2 with their distributions identified from monitoring data. As a result, the predicted expansion joint displacement at any given temperature from this model is not a deterministic value but rather a probability distribution. In practice, we are mainly concerned with the probability of failure when a new set of measurements is obtained. A performance indicator, named anomaly index, is defined herein to evaluate the failure probability of the expansion joint in the light of new measurement data. For any structural component, the probability of failure is defined as the probability of violating any of its limit states [34,35]. A limit-state function can be written as

$$g = R - S \tag{17}$$

where R is the capacity of displacement of the expansion joint under a certainty temperature, and S is the actual (measured) displacement response at the same temperature. The above function returns a negative value under failure conditions (i.e., $g < 0$) and a positive value when the system is healthy (i.e., $g > 0$); the limit state (i.e., $g = 0$) separates the safe region from the failure region. With the limit-state function, the probability of failure can be expressed as

$$P_f = P(g < 0) = P(R - S < 0) = \int_{-\infty}^{0} F_R(x) f_S(x) dx \tag{18}$$

where $F_R(x)$ is the cumulative distribution function (CDF) of the capacity and $f_S(x)$ is the probability density function (PDF) of the measured displacement. If R and S are independent normal variates, the failure probability can be determined as

$$P_f = \Phi\left(-\frac{\mu_R - \mu_S}{\sqrt{\sigma_R^2 + \sigma_S^2}}\right) \tag{19}$$

where $\Phi(\cdot)$ is a standard normal probability function; μ_R and μ_S are the means of R and S; and σ_R^2 and σ_S^2 are the standard variances of R and S. Akin to the safety index in reliability analysis, the anomaly index is defined as

$$\lambda = |\Phi^{-1}(P_f)| = \frac{|\mu_R - \mu_S|}{\sqrt{\sigma_R^2 + \sigma_S^2}} \tag{20}$$

where $\Phi^{-1}(\cdot)$ is the inverse of the standard normal cumulative distribution function. When new monitoring data are collected successively (e.g., month-by-month or year-by-year), the anomaly index can be evolutionarily evaluated by repeatedly using Eqs. (19) and (20).

3. Application to a long-span cable-stayed bridge

3.1. Ting Kau Bridge

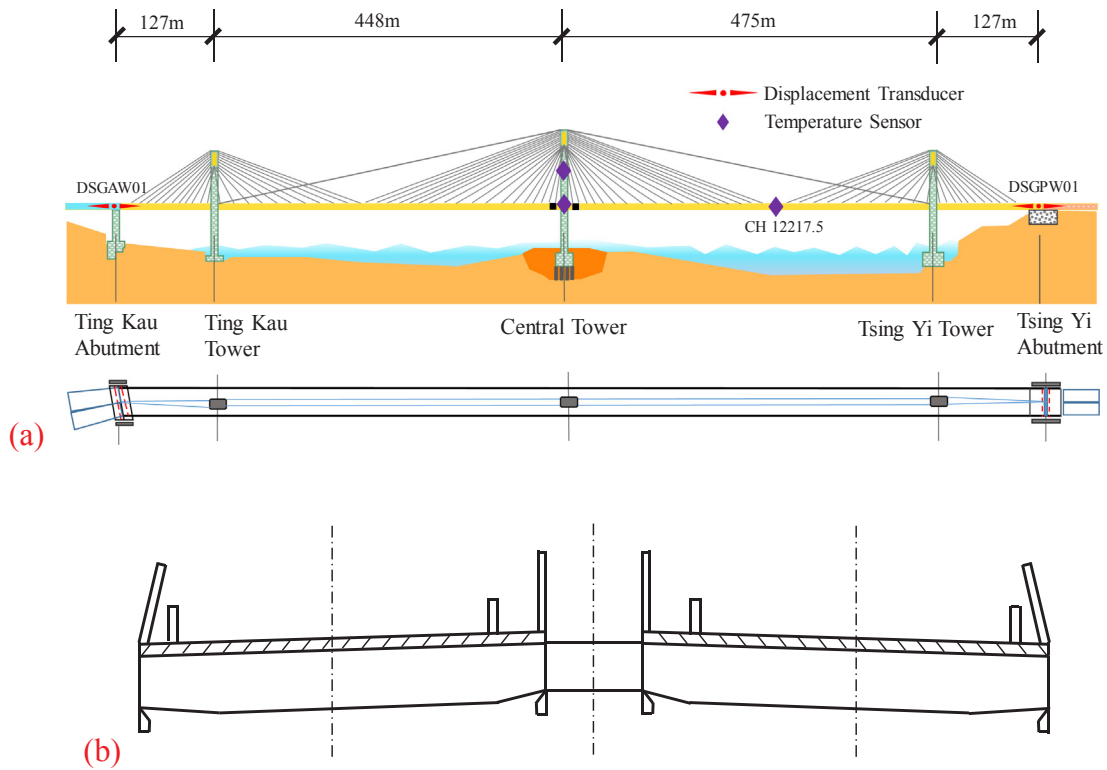The Ting Kau Bridge (TKB) in Hong Kong (Fig. 1) is a three-tower

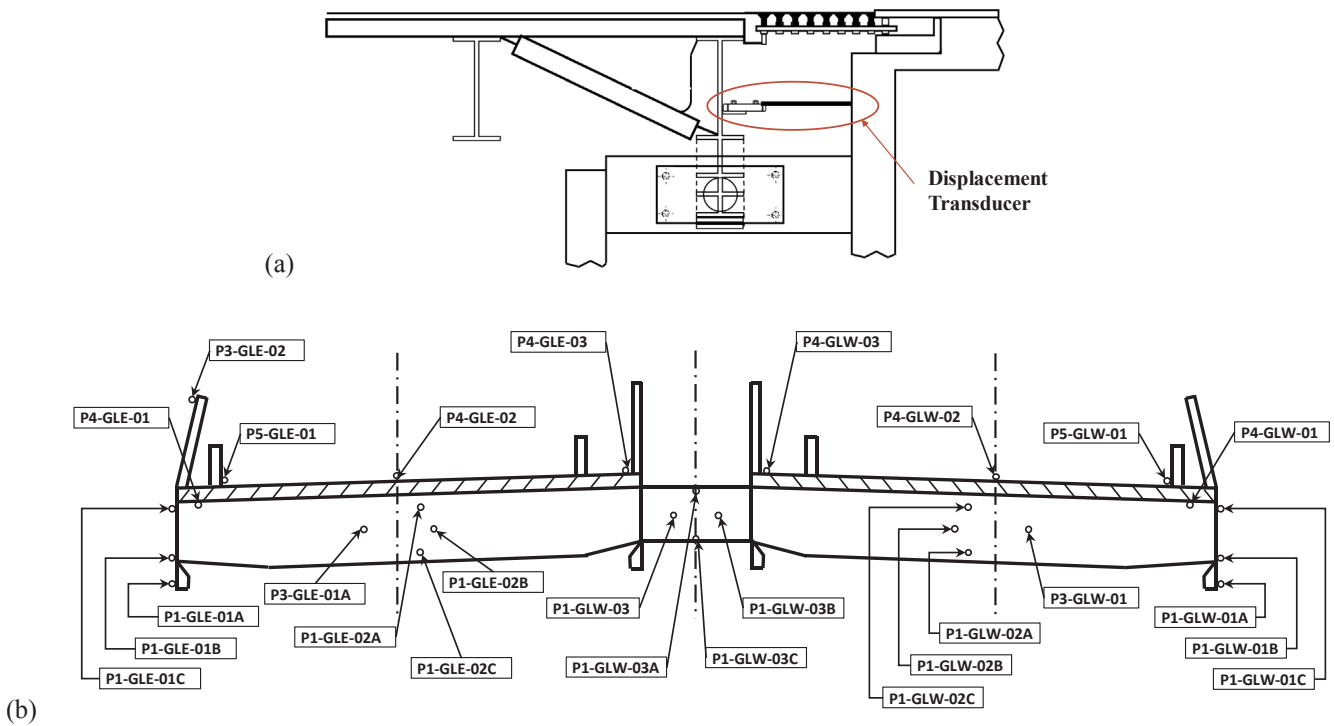**Fig. 1.** Ting Kau Bridge: (a) elevation; (b) deck cross-section.

Fig. 2. Layout of sensors on Ting Kau Bridge: (a) displacement transducer at Tsing Yi abutment; (b) temperature sensors on deck cross-section.

cable-stayed bridge with two main spans of 448 m and 475 m respectively, and two side spans of 127 m each [36]. The bridge deck is separated into two carriageways with a width of 18.8 m each, between them being three slender single-leg towers with respective heights of 170 m, 194 m, and 158 m. The deck is supported by 384 stay cables in four cable planes. A long-term SHM system comprising more than 230 sensors permanently installed on the TKB has been implemented by the

Hong Kong SAR Government Highways Department after completion of the bridge construction in 1999 [37,38]. The sensors deployed on the bridge include accelerometers, strain gauges, displacement transducers, anemometers, temperature sensors, GPS, and weigh-in-motion sensors [39,40]. Two displacement transducers (denoted as DSGAW01 and DSGPW01 in Fig. 1) have been used for the measurement of longitudinal movements of the expansion joints at both ends of the

continuous bridge deck. For the measurement of temperature in steel, concrete, asphalt and atmosphere, a total of 83 temperature sensors have been installed, of which 51 are deployed at one deck cross-section (i.e., CH 12217.5). The sampling rates of displacement transducers and temperature sensors are 2.56 Hz and 0.07 Hz, respectively. Fig. 2 illustrates the deployment of a displacement transducer at the Tsing Yi abutment (i.e., DSGPW01) and the temperature sensors on the heavily instrumented deck cross-section (i.e., CH12217.5).

3.2. Monitoring data of displacement and temperature

One-year continuous monitoring data of the TKB in its intact stage, including the displacements at two expansion joints (DSGAW01 and DSGPW01) and the temperatures on the heavily instrumented deck cross-section (CH12217.5), are employed to formulate the Bayesian DTR model. The measured temperatures from 39 sensors on the cross-section, including 15 in steel and 24 in concrete, are used to calculate the effective temperature. By dividing the cross section into 39 sub-areas, the effective temperature is estimated by Eq. (2) making use of the measured temperatures from the 39 sensors. The hourly-average displacements and effective temperatures are utilized as the target quantities. Before embarking on Bayesian regression modelling, the one-year monitoring data were carefully screened to identify outliers and eliminate any unrealistic values, e.g., abnormal data caused by malfunctioning of the acquisition equipment. A total of 3511 h of data were finally selected for the regression modelling, in which the first 2891-hour data representing the healthy state of the expansion joints were chosen as the training dataset in Bayesian DTR modelling, while the remaining 720-hour (corresponding to one month) data representing unknown state of the expansion joints were used as testing dataset for model validation. Fig. 3 shows the data sequence of the hourly-average effective temperature and expansion joint displacements measured in one year.

After obtaining the effective temperature and displacement, a check on the relationship between the displacement of expansion joints and the effective temperature of bridge deck was made. Fig. 4 shows the effective temperature and expansion joint displacements at the Ting Kau and Tsing Yi abutments for a duration of 48 h, where DSGAW01 denotes the displacement at the Ting Kau abutment and DSGPW01 denotes the displacement at the Tsing Yi abutment. It is seen that the variation of displacements coincides well with effective temperature fluctuation.

3.3. Formulation of Bayesian DTR model

Since only one covariate (i.e., effective temperature) is considered in the Bayesian DTR modelling, the regression model reduces to

$$y_\alpha = \beta_1 x_{\alpha 1} + \beta_2 x_{\alpha 2} + \varepsilon_\alpha, \quad \alpha = 1, \cdots, n \qquad (21)$$
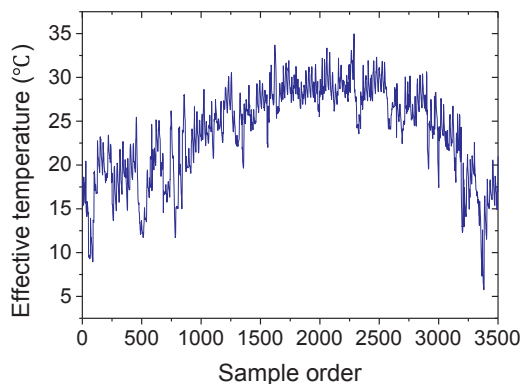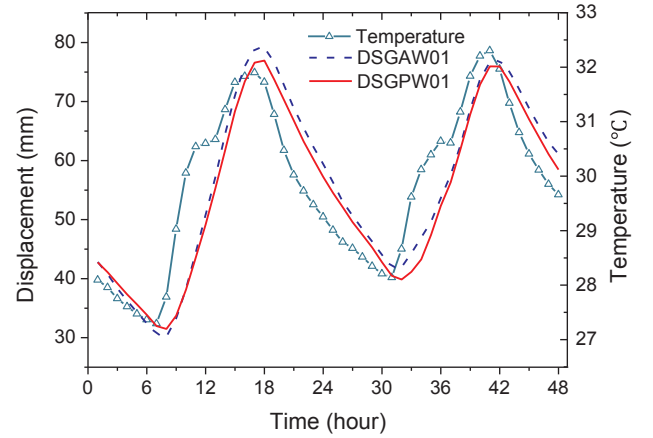

Fig. 4. Time history of displacements and effective temperature.

where y_α represents the hourly-average displacement of an expansion joint; $x_{\alpha 1}$ is implicitly set to 1 to allow for an intercept; $x_{\alpha 2}$ denotes the hourly-average effective temperature; and ε_α is the regression error.

3.3.1. Selection of prior distribution

To implement the Bayesian inference to regression analysis, prior distribution for each model parameters should be specified. In this study, the Normal Inverse-Gamma prior is adopted to depict the conjugate prior of the model parameters, which is expressed as

$$f(\boldsymbol{\beta}, \sigma^2) = f(\boldsymbol{\beta}|\sigma^2) \times f(\sigma^2) = N\left(0, \sigma^2 \sum\nolimits_0\right) \times IG\left(\frac{a}{2}, \frac{b}{2}\right) \qquad (22)$$

The level of (un)certainty in a prior is manipulated through the specified features of the prior distribution, and these features are called hyperparameters in the Bayesian context. For example, a normal distribution is defined through a mean and a variance, so the amount of knowledge incorporated into normal distribution is directly controlled by the mean and variance hyperparameters. Fig. 5 shows four normal distributions having different values of the variance hyperparameter. It can be seen that the distributions with small variance (1 and 10) illustrate much more certainty about the possible values of the parameter because the spread of these distributions covers a much smaller range of possible values than those plots with large variance. In other words, the distributions with large variance (100 and 1000) bear very little certainty about the possible values of the parameter because there are much larger spreads of possible values.

Akin to normal distributions, inverse-gamma distributions with different parameter values are also manipulated as shown in Fig. 6. In general, the parameters a and b dictate the possible range of values for the corresponding parameters being estimated. The smaller the values of a and b, the larger the spread of the possible values.
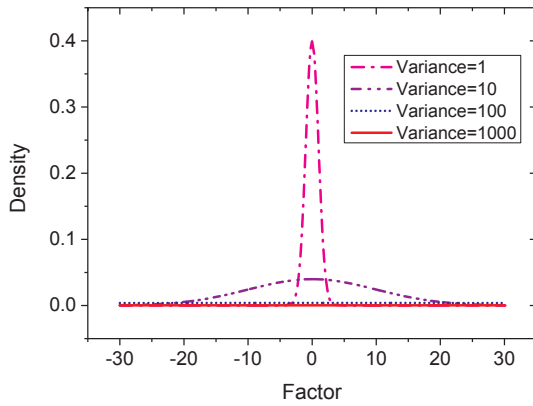

Fig. 3. Sequence of measured effective temperature and expansion joint displacements.
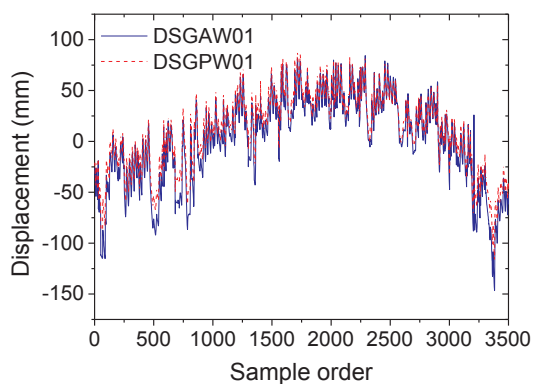
Fig. 5. Prior distribution illustrating different levels of informativeness (Normal).
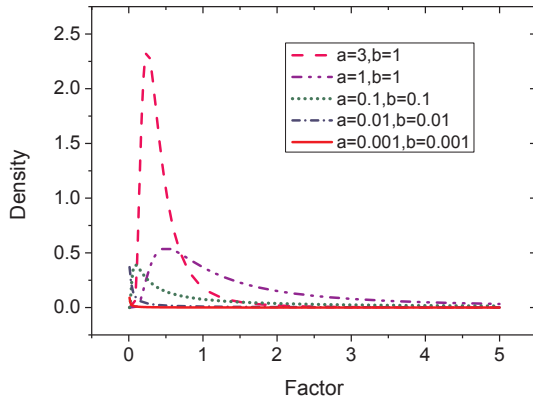

Fig. 6. Prior distribution illustrating different levels of informativeness (Inverse-Gamma).

Because of the very little certainty of the parameters, we chose the prior distribution parameters enabling to cover a wide range of the possible values. Herein, we set $\sum_0 = 1000 \times I_2$ (I_2 is two-dimensional unit matrix), and $a = b = 0.001$, which makes the prior distribution highly diffuse.

3.3.2. Estimation of model parameters

Both analytical solution and Gibbs sampler are applied to elicit the posterior distributions of $\boldsymbol{\beta}$ (i.e., β_1 and β_2) and σ^2. It is necessary to check that the generated posterior samples are resulting from a stationary distribution to ensure the accuracy of the results. Both trace plot and convergence diagnostic are used here to examine the convergence of Gibbs iterations. The total number of iterations was chosen as 25,000, of which the first 20,000 iterations were discarded while the last 5,000 posterior samples left for parameter estimation after convergence checking.

The left panels in Fig. 7 show the sample paths of the retained 5,000 draws for Model 1 (the expansion joint at Ting Kau abutment). As illustrated, there is no evidence of a lack of convergence from the trace plots. The values of convergence diagnostic for the estimated model parameters are all close to zero (between -0.029 and 0.025), indicating that the posterior samples meet the convergence requirement. The right panels in Fig. 7 show the posterior distributions of the model parameters with 95% confidence interval (the blue area). Similarly, the sample paths and posterior densities of the model parameters for Model 2 (the expansion joint at Tsing Yi abutment) are presented in Fig. 8.

Due to the statistical nature of the Bayesian approach, more detailed information about the model parameters, such as posterior mean, Standard Deviation (SD), 95% posterior confidence interval, skewness and kurtosis, can all be obtained from the retained 5,000 samples, as

illustrated in Table 1. The results from both analytical solution and Gibbs sampler are given. It is found that the approximate results are pretty much the same as the analytical results, verifying the accuracy of the Gibbs sampler method. The SD is a measure that quantifies the uncertainty of each parameter. In both Models 1 and 2, β_2 has the lowest SD value (0.03 for both), β_1 comes second (0.75 and 0.72), and model error σ^2 owns the largest SD value (2.24 and 2.03), which implies the model error σ^2 has a higher uncertainty than β_1 and β_2. As shown in the table, the values of skewness are nearly zero and kurtosis are close to 3, indicating that the estimated posterior densities are approximately normal distribution.

The mean slopes of the Bayesian DTR models are 7.93 and 6.88 mm/°C for the expansion joints at the Ting Kau abutment and the Tsing Yi abutment, respectively. As the expansion lengths for spans on the left and right sides of the central tower are 575 m and 602 m, the thermal expansion coefficients can be estimated to be 13.79×10^{-6} per °C and 11.43×10^{-6} per °C, which are close to the design value of 12.0×10^{-6} per°C. For the purpose of comparison, the conventional deterministic linear regression models are also formulated by using the same set of data. It is obtained that the slopes of the deterministic linear regression models are 8.04 mm/°C for the Ting Kau abutment and 7.07 mm/°C for the Tsing Yi abutment. Hence the corresponding expansion coefficients are calculated to be 13.98×10^{-6} per °C and 11.74×10^{-6} per °C, respectively, which are close to the results estimated by the Bayesian DTR models.

Fig. 9 shows the correlation between the expansion joint displacement and effective temperature for both expansion joints. As mentioned before, the estimated correlation model is in distribution form. For illustration, five probability distributions of the displacement as regards five specific temperatures (10 °C, 15 °C, 20 °C, 25 °C and 30 °C) are provided. Also plotted is the mean of the estimated displacements (red line), which agrees well with the measurements. Compared to the traditional regression modelling, an appealing advantage of the Bayesian regression modelling is that the model error can be quantitatively estimated in conjunction with model parameters, making the model interpretation more reasonable. From Table 1, it is seen that Model 2 has a smaller model error than Model 1, which indicates that Model 2 is relatively more accurate under the assumption that the monitoring data from the two expansion joints contain the same level of contaminated noise in statistical sense.

3.3.3. Evaluation of prediction capability

The prediction capability of the formulated Bayesian DTR models is then evaluated using the testing dataset. By transforming the raw temperature data into hourly-average effective temperature, the displacements of expansion joints DSGAW01 and DSGPW01 are estimated from their corresponding Bayesian DTR models by inputting the effective temperatures. The forecast mean displacements with 95% confidence interval generated by the Bayesian DTR models are shown in Fig. 10, where the measured counterparts are also presented for comparison. It is seen that the predicted displacements coincide well with the measurements in both training and testing phases. The prediction errors are provided in Fig. 11. It is observed that there is almost no deviation in prediction errors between the training and testing phases. To quantify the discrimination and forecast capability, two performance metrics, Root Mean Squared Error (RMSE) and Mean Likelihood (ML), are calculated. They are defined as

$$\text{RMSE} = \sqrt{\frac{1}{n} \sum_{i=1}^{n} (y_i - \mu_{y_i})^2}$$

(23)

$$\text{ML} = \frac{1}{n} \sum_{i=1}^{n} p(y_i | \mu_{y_i}, \sigma_{y_i}^2)$$

(24)

where y_i is the measured displacement; μ_{y_i} and $\sigma_{y_i}^2$ are predictive mean and variance of displacement, respectively. The RMSE quantifies the
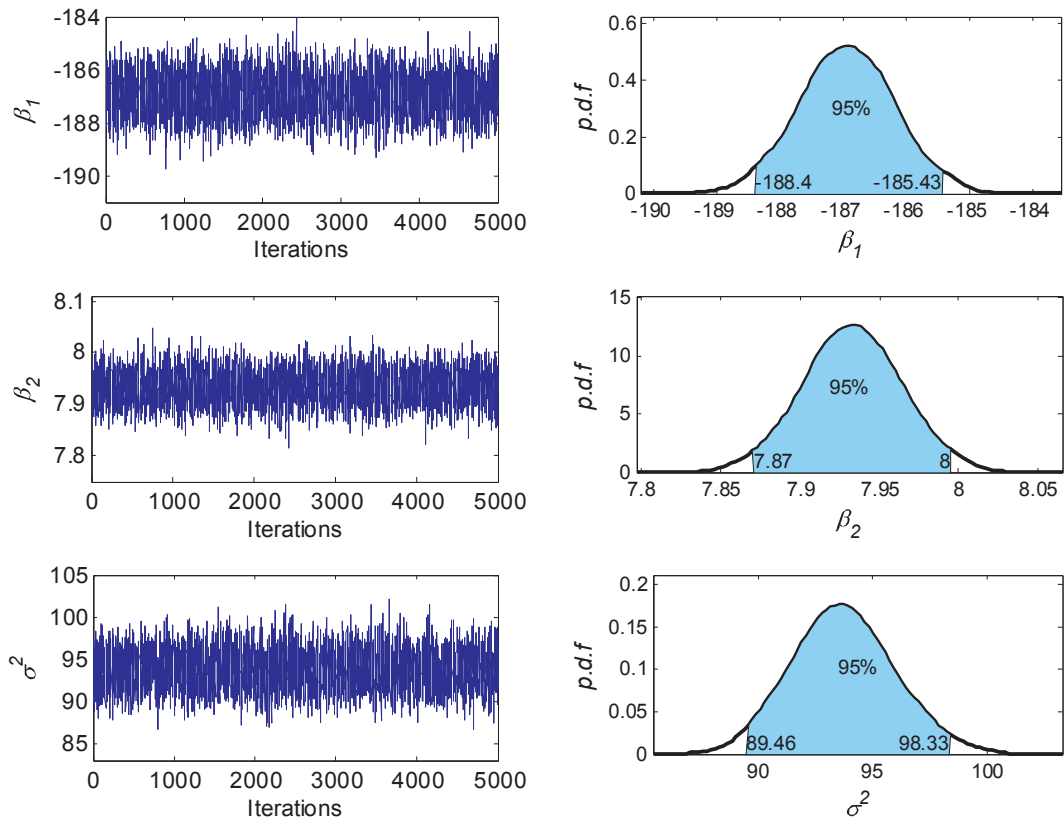
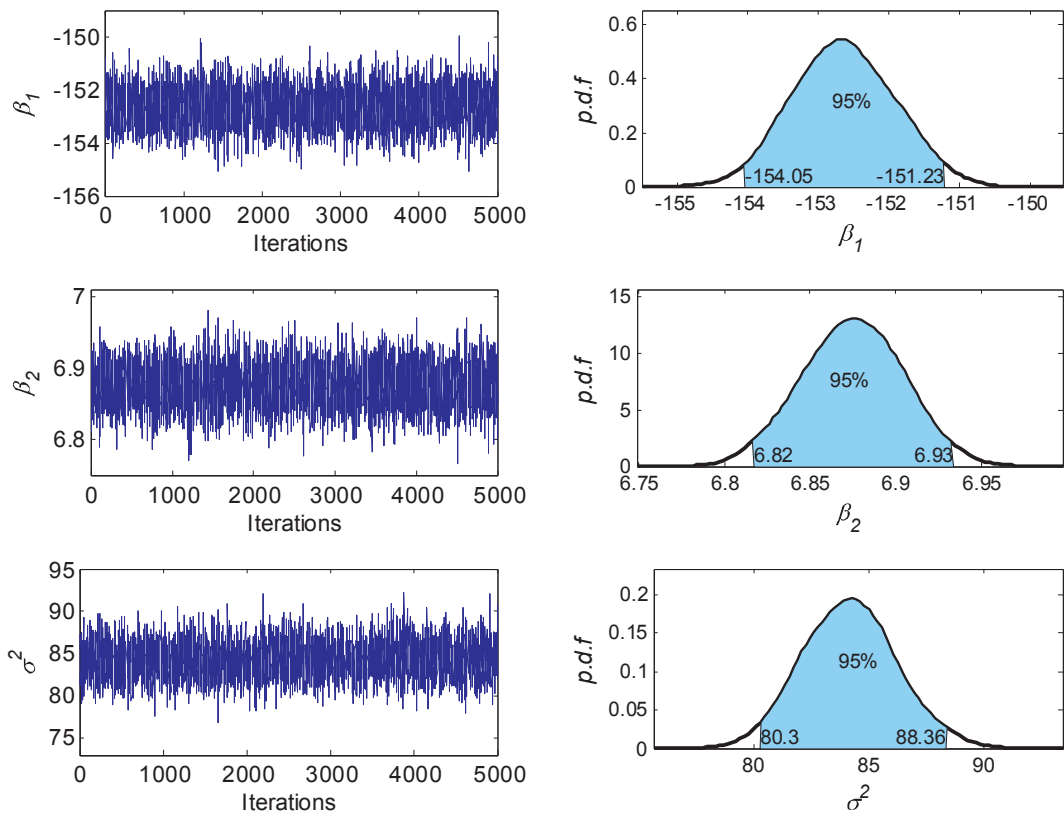**Fig. 7.** Sample paths and estimated posterior densities for parameters (Ting Kau abutment).

Fig. 8. Sample paths and estimated posterior densities for parameters (Tsing Yi abutment).

Table 1
Summary of model parameters.

Expansion joint		Mean		SD		95% confidence interval	Skewness	Kurtosis
		Analytical	Gibbs	Analytical	Gibbs			
Ting Kau abutment	β_1	−186.88	−186.94	0.75	0.75	[−188.40, −185.43]	−0.01	2.98
	β_2	7.92	7.93	0.03	0.03	[7.87, 8.00]	−0.005	2.97
	σ^2	93.69	93.70	2.24	2.26	[89.46, 98.33]	0.15	2.97
Tsing Yi abutment	β_1	−152.83	−152.65	0.72	0.73	[−154.05, −151.23]	0.04	2.92
	β_2	6.88	6.88	0.03	0.03	[6.82, 6.93]	−0.03	2.93
	σ^2	84.03	84.18	2.03	2.03	[80.30, 88.36]	0.13	3.06

Fig. 9. Formulated Bayesian DTR models: (a) DSGAW01; (b) DSGPW01.

Fig. 10. Comparison between measured and estimated displacements of expansion joints for training dataset and testing dataset: (a) DSGAW01; (b) DSGPW01.

Fig. 11. Estimation error for training dataset and testing dataset: DSGAW01; (b) DSGPW01.
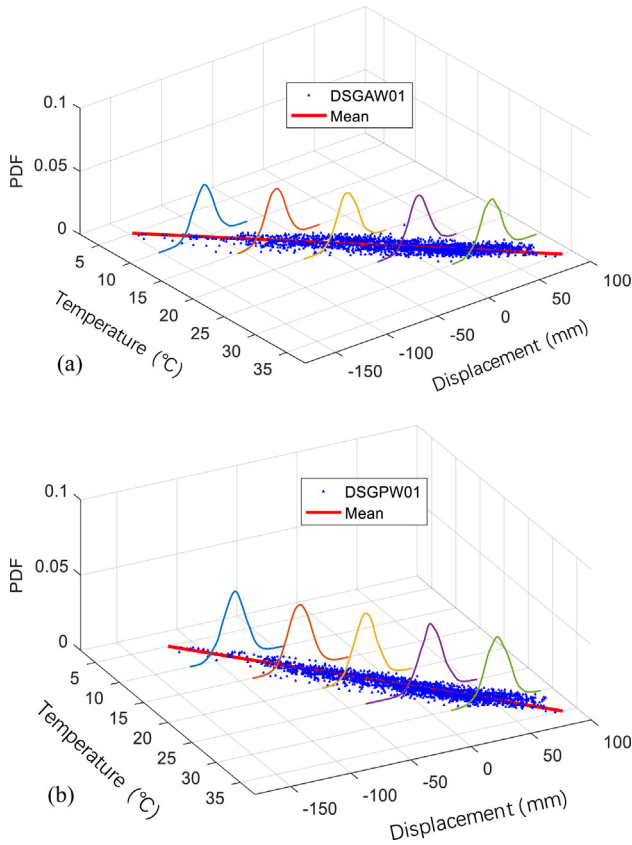
overall accuracy of forecasts, whereas the ML measures the probability of the measurements that are reproduced by the forecasts. The lower the value of RMSE and the higher the magnitude of ML, the more precise the results generated by the model [41]. The results of RMSE and ML for the training and testing phases are provided in Fig. 12. It is evident that for both performance metrics there is no significant distinction between the training and testing phases. It proves once again that the formulated models are competent to characterize and predict the displacement-temperature relationship.

The results of the RMSE metric for the Bayesian DTR models and the deterministic linear regression models are listed in Table 2. By comparing the two sets of data, it can be found that the forecasting performance of the Bayesian DTR models is superior to that of the deterministic linear regression models in both training and testing phases.

3.3.4. Prediction of extreme displacement

One general objective of SHM is to verify or validate design parameters with the use of real-world monitoring data. According to the design documents of the T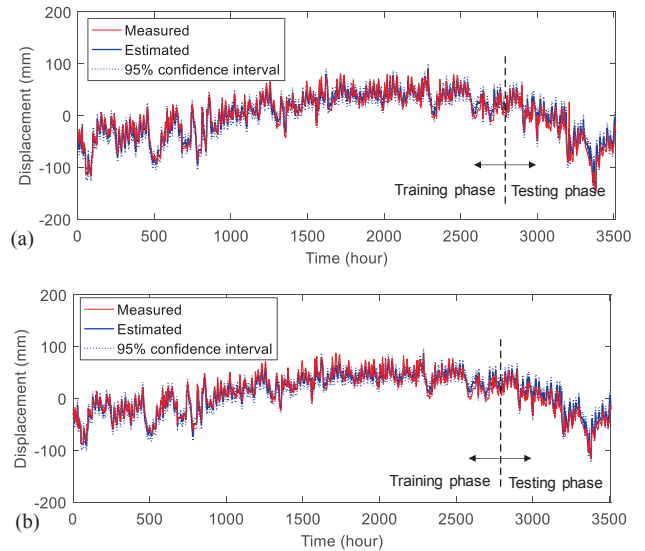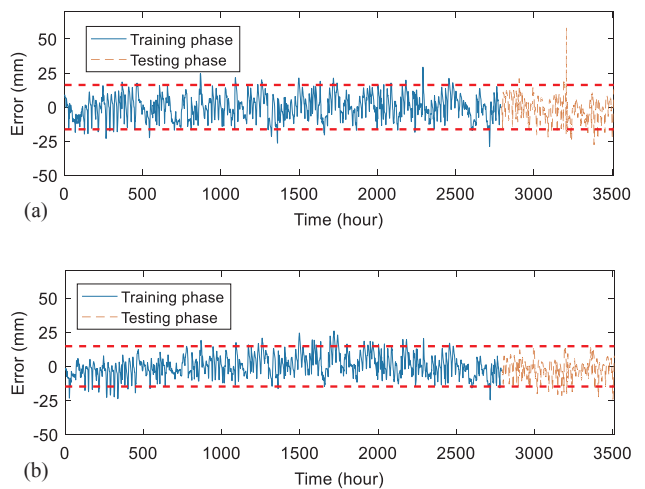KB, the maximum and minimum design temperatures are 40 °C and −2 °C, respectively [42]. Substituting the design values into the formulated Bayesian DTR models, the corresponding predictive distributions about the maximum and minimum displacements are obtained as shown in Figs. 13 and 14.

The means, SDs and 95% posterior confidence intervals of the predicted displacements at the maximum and minimum design temperatures are summarized in Table 3. According to the predicted mean
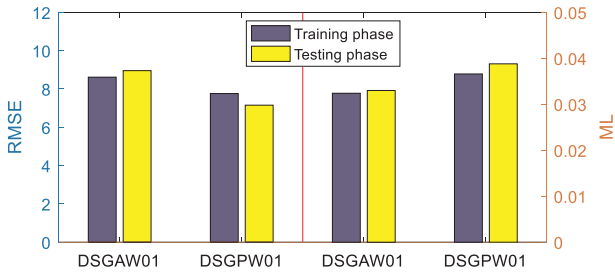
Fig. 12. Comparison of prediction performance for training dataset and testing dataset.

Table 2
Comparison of Bayesian DTR models and deterministic linear regression models in terms of forecasting performance.

	DSGAW01		DSGPW01	
	Training phase	Testing phase	Training phase	Testing phase
Bayesian DRT models	8.50	9.04	7.69	7.20
Deterministic linear regression models	9.15	9.13	8.41	7.34

displacements at the maximum and minimum temperatures, the mean displacement ranges (difference between the predicted mean displacements at the maximum and minimum temperatures) are 332.68 mm at the Ting Kau abutment and 290.19 mm at the Tsing Yi abutment, respectively, which are very close to the design values of 339 mm and 297 mm [8]. The discrepancy between the predicted and design values is smaller than the SD. However, the displacement ranges with 95% confidence interval are [298.52, 371.37] at the Ting Kau abutment and [252.99, 325.26] at the Tsing Yi abutment, whose upper bounds exceed the design criterion. It would be considered in the future renovation of the expansion joints.

Similarly, by substituting the design temperature values into the deterministic linear regression models, the displacement range of the expansion joints, due to temperature variation, is obtained to be 336.29 mm at the Ting Kau abutment and 293.14 mm at the Tsing Yi abutment, respectively. Both are in coincidence with the results elicited from the Bayesian DTR models.

3.3.5. Verification for anomaly detection

The Bayesian DTR models formulated under the intact state of expansion joints can be used to represent a normal correlation pattern, which will break down if the performance of the expansion joints degrades. With the established correlation pattern, anomaly alarms will be issued if the future longitudinal displacement disobeys the normal pattern. According to the literature [1,43], the common joint defects which affect the longitudinal displacement include: (i) restriction of freedom of joint movement; (ii) impact of rotation, tilting, or settlement; (iii) accumulation of debris and incompressible materials in the seals; and (iv) loose, rusted, cracked, missing, or damaged steel plates and so forth. Making use of the longitudinal displacement monitoring

data, the proposed anomaly index for damage alarm is examined.

To illustrate how the proposed method performs condition assessment and damage alarm under different perturbations, the expansion joint displacements at the temperature of 30 °C is considered as an example. The predictive distributions in expansion joint displacements are obtained by substituting the temperature 30 °C into the Bayesian DTR models, where the means of the predicted displacements are 51.46 mm for DSGAW01 and 53.84 mm for DSGPW01. To simulate different degrees of damage, the measured displacements at 30 °C are assumed to be 10, 20, 30, 40, 50, 60, 70, 80 and 90 mm for both expansion joints. Then the anomaly index characterizing the deviation of the measured displacements from the model predictions is evaluated according to Eq. (20). As illustrated in Fig. 15, the more the measured displacement deviates from the predicted displacement (red pentagram), the bigger the anomaly index, which means the higher probability of failure on expansion joint. Thus, the degree of failure can be graded in terms of the value of anomaly index. The 95% confidence level (red dotted line) can be considered as a threshold for quick anomaly detection. The expansion joint will be flagged as abnormal once the anomaly index exceeds the threshold.

To verify the efficacy of the proposed method for damage alarm, four degradation cases in terms of different drifts are considered for both expansion joints DSGAW01 and DSGPW01. The degradation severities in the four cases are shown in Table 3, where Case 1 represents the intact state and the other three cases (with an offset of 10, 20 and 30 mm from the original measured displacements in testing phase, respectively) represent three different degradation conditions. The corresponding degradation rates are respectively 0%, 2.9%, 5.9% and 8.8% for the expansion joint DSGAW01, and 0%, 3.3%, 6.7% and 10.1% for the expansion joint DSGPW01. The capability of damage alarm, using 95% confidence level as control limits, is evaluated in terms of alarm rate, which is defined as the percentage of the number of alarms relative to the total number of testing data. One advantage of using the alarm rate is that it helps avoid false-positive alarm caused by spikes in the monitoring data, since the percentage of spikes/outliers is often too low to generate a large alarm rate. The results obtained by the proposed method in relation to different degrees of degradation are provided in Table 4. It is observed that damage alarm is triggered more frequently as degradation is incrementally aggravated. More specifically, only a few samples trigger alarm (the alarm rate is less than 8%) in Case 1 (no drift), whereas nearly all the samples trigger alarm (the alarm rate is nearly 100%) in Case 4 (a drift of 30 mm). Fig. 16 illustrates the values of anomaly index in the training and testing phases for Case 1. It is seen that almost no deviation occurs in the anomaly index between the training and testing phases, implying that the condition of the expansion joints in the testing phase is healthy. However, for Case 4 as shown in Fig. 17, the values of anomaly index in the testing phase deviate apparently from those in the training phase and are remarkably higher than the threshold. As a result, the proposed method performs favorably in assessing the performance and health condition of expansion joints.

It is worth mentioning that this study assumes that the longitudinal displacement of the expansion joints is mainly due to temperature variations without considering other factors. In reality, strong winds
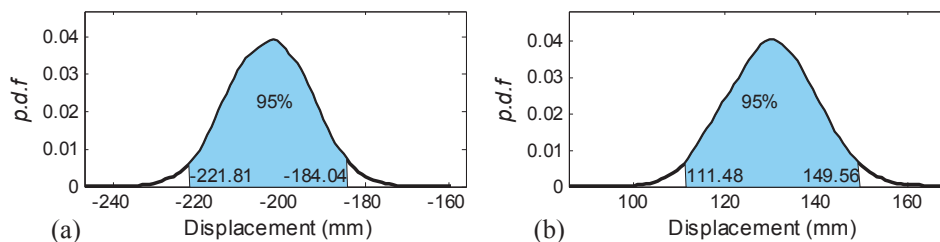

Fig. 13. Predictive distribution of expansion joint displacement (DSGAW01) at the maximum and minimum design temperatures: (a) −2 °C; (b) 40 °C.
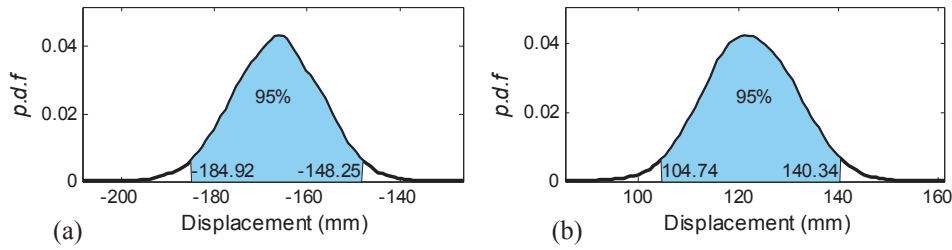
Fig. 14. Predictive distribution of expansion joint displacement (DSGPW01) at the maximum and minimum design temperatures: (a) −2 ℃; (b) 40 ℃.

Table 3
Predicted displacements at the maximum and minimum design temperatures.

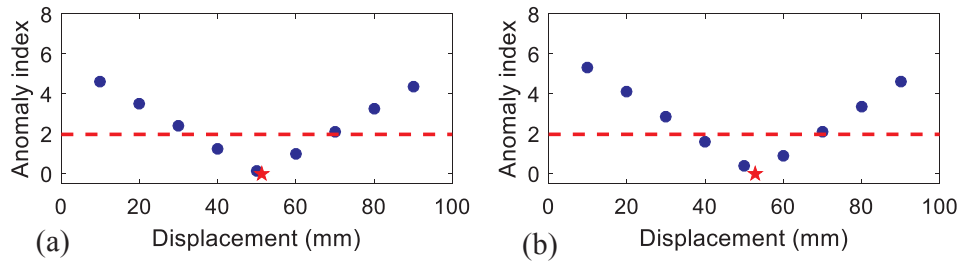| Expansion joint	T (℃)	Mean (mm)		SD		95% confidence interval (mm)	Mean range (mm)
		Analytical	Gibbs	Analytical	Gibbs		
DSGAW01	−2	−202.66	−202.78	9.84	9.76	[−221.81, −184.04]	332.68
	40	130.02	130.24	9.82	9.81	[114.48, 149.56]	
DSGPW01	−2	−167.42	−166.50	9.08	9.31	[−184.92, −148.25]	290.19
	40	122.77	122.38	9.06	9.12	[104.74, 140.34]	

Fig. 15. Anomaly index for different abnormal cases: (a) DSGAW01; (b) DSGPW01.

Table 4
Damage alarm in different degradation cases.

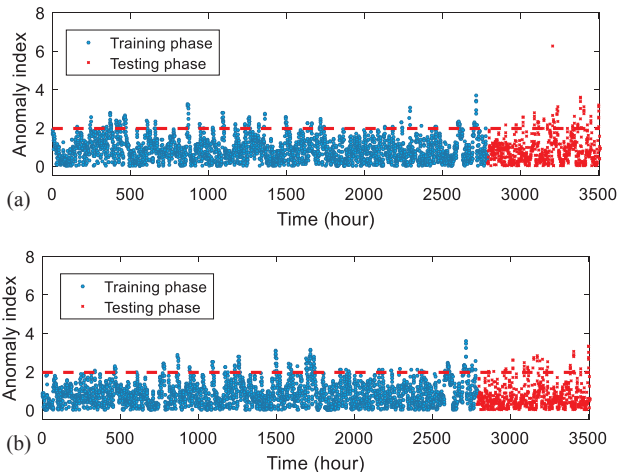| Case	Degradation severity (mm)	DSGAW01		DSGAW01	
		Number of alarms	Alarm rate (%)	Number of alarms	Alarm rate (%)
1	0	56	7.78	44	6.11
2	10	350	48.61	452	62.78
3	20	633	87.92	690	95.83
4	30	717	99.58	720	100

Fig. 16. Anomaly index in training and testing phases for Case 1: DSGAW01; (b) DSGPW01.
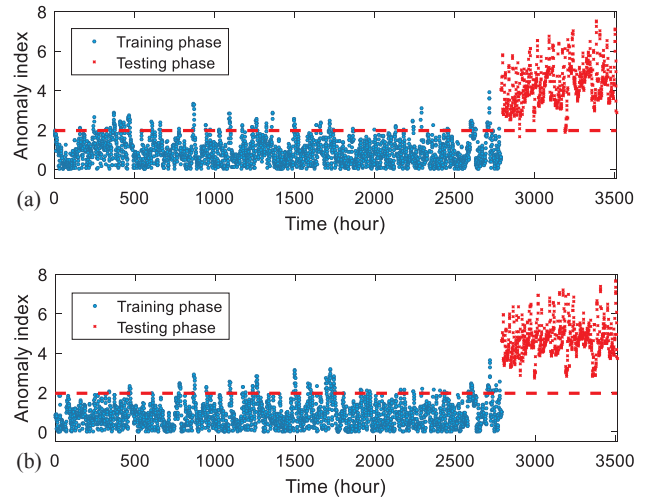

Fig. 17. Anomaly index in training and testing phases for Case 4: (a) DSGAW01; (b) DSGPW01.

and heavy traffic may also induce changes of the longitudinal displacement to some extent. However, the wind- and traffic-induced longitudinal displacement is merely a second-order effect and short-lived, and the longitudinal displacement will return to normal after the loads are removed. An advantage of the Bayesian DTR model is that it can account for various uncertainties including the effect of wind and traffic loads.

4. Summary and conclusions

In this study, a probabilistic method in the context of Bayesian inference is proposed for SHM-based condition assessment and damage alarm of bridge expansion joints. In the formulated Bayesian DTR model, the model parameters are considered as random variables with their distributions identified from monitoring data, and thus the model can explicitly account for uncertainties arising from measurement noise, environmental variability and model error. Moreover, the proposed method enables to quantify the prediction uncertainty in foreseeing the future observation with newly collected monitoring data. The formulated model in the Bayesian context is seamlessly in compliance with the anomaly index elicited in the context of reliability theory. To facilitate general Bayesian inference, both analytical solution for natural conjugate prior and Gibbs sampler algorithm for non-conjugate prior are provided.

The proposed method has been verified by use of long-term monitoring data acquired from a long-span cable-stayed bridge. The case study comes to the following observations: (i) The formulated Bayesian DTR models characterize well the correlation between the displacement of expansion joints and the effective temperature of bridge deck, with the uncertainties duly reflected in the random model parameters and error parameter. The estimated posterior densities of the model parameters and error are approximately normal distributions; (ii) The formulated Bayesian DTR models perform as good in prediction (testing phase) as in reproduction (training phase), with the forecasting capability validated in terms of both RMSE and ML. The predicted extreme displacements of the two expansion joints by the Bayesian DTR models at the maximum and minimum design temperatures are highly coincident with the design values, validating the design assumptions; and (iii) The proposed anomaly index is capable to evaluate the probability of failure of expansion joints when new measurement is available. The bigger the anomaly index, the higher the probability of failure of the expansion joints. When the degradation due to draft exceeds a certain value (e.g., 10 mm), the alarm rate resulting from the anomaly index is significantly increased, signaling the occurrence of potential damage. Also, using the alarm rate helps to avoid the false-positive alarm caused by spikes in the monitoring data.

CRediT authorship contribution statement

Y.Q. Ni: Conceptualization, Methodology, Resources, Writing - review & editing, Supervision, Project administration, Funding acquisition. **Y.W. Wang:** Software, Formal analysis, Investigation, Writing - original draft, Visualization. **C. Zhang:** Data curation, Validation.

Declaration of competing interest

The authors declare that they have no known competing financial interests or personal relationships that could have appeared to influence the work reported in this paper.

Acknowledgements

Appendix A. Supplementary material

Supplementary data to this article can be found online at https://doi.org/10.1016/j.engstruct.2020.110520.

References

[1] Chang LM, Lee YJ. Evaluation of performance of bridge deck expansion joints. J Performance Constructed Facilities (ASCE) 2002;16(1):3–9.
[2] Roeder CW. Fatigue and dynamic load measurements on modular expansion joints. Constr Build Mater 1998;12(2):143–50.
[3] Lima JM, de Brito J. Inspection survey of 150 expansion joints in road bridges. Eng Struct 2009;31(5):1077–84.
[4] Guo T, Liu J, Zhang Y, Pan S. Displacement monitoring and analysis of expansion joints of long-span steel bridges with viscous dampers. J Bridge Eng (ASCE) 2014:04014099.
[5] Okuda M, Yumiyama S, Ikeda H. Reinforcement of expansion joint on Akashi Kaikyo Bridge. In: JSCE 59th Annual Meeting, Japan Society of Civil Engineers 2004, Tokyo [in Japanese].
[6] Sun Z, Zhang Y. Failure mechanism of expansion joints in a suspension bridge. J Bridge Eng (ASCE) 2016;21(10):05016005.
[7] Coelho BZ, Vervuurt AHJM, Peelen WHA, Leendertz JS. Dynamics of modular expansion joints: the Martinus Nijhoff bridge. Eng Struct 2013;48:144–54.
[8] Ni YQ, Hua XG, Wong KY, Ko JM. Assessment of bridge expansion joints using long-term displacement and temperature measurement. J Performance f Constructed Facilities (ASCE) 2007;21(2):143–51.
[9] Ding Y, Li A. Assessment of bridge expansion joints using long-term displacement measurement under changing environmental conditions. Front Archit Civ Eng China 2011;5(3):374–80.
[10] Huang HB, Yi TH, Li HN, Liu H. New representative temperature for performance alarming of bridge expansion joints through temperature-displacement relationship. J Bridge Eng (ASCE) 2018;23(7):04018043.
[11] Alvin K. Finite element model update via Bayesian estimation and minimization of dynamic residuals. AIAA J 1997;35(5):879–86.
[12] Beck JL, Katafygiotis LS. Updating models and their uncertainties. I: Bayesian statistical framework. J Eng Mech (ASCE) 1998;124(4):455–61.
[13] Katafygiotis LS, Beck JL. Updating models and their uncertainties. II: Model identifiability. J Eng Mech (ASCE) 1998;124(4):463–7.
[14] Beck JL, Yuen KV. Model selection using response measurements: Bayesian probabilistic approach. J Eng Mech (ASCE) 2004;130(2):192–203.
[15] Lam HF, Ng CT. The selection of pattern features for structural damage detection using an extended Bayesian ANN algorithm. Eng Struct 2008;30(10):2762–70.
[16] Goller B, Schueller GI. Investigation of model uncertainties in Bayesian structural model updating. J Sound Vib 2011;330(25):6122–36.
[17] Yuen KV, Mu HQ. Real-time system identification: an algorithm for simultaneous model class selection and parametric identification. Comput-Aided Civ Infrastruct Eng 2015;30(10):785–801.
[18] Zhang FL, Ni YQ, Ni YC, Wang YW. Operational modal analysis of Canton Tower by a fast frequency domain Bayesian method. Smart Struct Syst 2016;17(2):209–30.
[19] Wang J, Liu XZ, Ni YQ. A Bayesian probabilistic approach for acoustic emission-based rail condition assessment. Comput-Aided Civ Infrastruct Eng 2018;33(1):21–34.
[20] Yang JH, Lam HF, Beck JL. Bayes-Mode-ID: A Bayesian modal-component-sampling method for operational modal analysis. Eng Struct 2019;189:222–40.
[21] Wagner PR, Fahrni R, Klippel M, Frangi A, Sudret B. Bayesian calibration and sensitivity analysis of heat transfer models for fire insulation panels. Eng Struct 2020;205:110063.
[22] Wang YW, Ni YQ, Wang X. Real-time defect detection of high-speed train wheels by using Bayesian forecasting and dynamic model. Mech Syst Sig Process 2020;139:106654.
[23] Zhou HF, Ni YQ, Ko JM. Constructing input to neural networks for modeling temperature-caused modal variability: mean temperatures, effective temperatures, and principal components of temperatures. Eng Struct 2010;32(6):1747–59.
[24] Lindley DV, Smith AFM. Bayes estimates for the linear model. J Roy Stat Soc: Ser B (Methodol) 1972;34(1):1–41.
[25] Ando T. Bayesian model selection and statistical modeling. New York: CRC Press; 2010.
[26] Alston CL, Mengersen KL, Pettitt AN. Case studies in Bayesian statistical modelling and analysis. New York: John Wiley & Son; 2012.
[27] Bishop CM. Pattern recognition and machine learning. New York: Springer; 2006.
[28] Raiffa H, Schlaifer R. Applied statistical decision theory. New York: John Wiley & Sons; 2000.
[29] Koop G. Bayesian econometric methods. New York: John Wiley & Sons; 2003.
[30] Gelfand AE, Smith AFM. Sampling-based approaches to calculating marginal densities. J Am Stat Assoc 1990;85(410):398–409.
[31] Feinberg SE, van der Linden WJ. Statistics for social and behavioral sciences. New York: Springer; 2005.
[32] Raftery AE, Lewis S. How many iterations in the Gibbs sampler. Bayesian Statist 1999;4(2):763–73.
[33] Depaoli S, Boyajian J. Linear and nonlinear growth models: describing a Bayesian perspective. J Consult Clin Psychol 2014;82(5):784–802.
[34] Frangopol DM. Life-cycle performance, management, and optimisation of structural systems under uncertainty: accomplishments and challenges. Struct Infrastruct Eng 2011;7(6):389–413.

[35] Xia HW, Ni YQ, Wong KY, Ko JM. Reliability-based condition assessment of in-service bridges using mixture distribution models. Comput Struct 2012;106–107:204–13.

[36] Bergermann R, Schlaich M. Ting Kau Bridge, Hong Kong. Struct Eng Int 1996;6(3):152–4.

[37] Wong KY. Instrumentation and health monitoring of cable-supported bridges. Struct Control Health Monit 2004;11(2):91–124.

[38] Ko JM, Ni YQ. Technology developments in structural health monitoring of large-scale bridges. Eng Struct 2005;27(12):1715–25.

[39] Wong KY. Design of a structural health monitoring system for long-span bridges. Struct Infrastruct Eng 2007;3(2):169–85.

[40] Ni YQ, Wong KY, Xia Y. Health checks through landmark bridges to sky-high structures. Adv Struct Eng 2011;14(1):103–19.

[41] Wan HP, Ni YQ. Bayesian modeling approach for forecast of structural stress response using structural health monitoring data. J Struct Eng (ASCE) 2018;144(9):04018130.

[42] Wong KY, Man DKL, Chan KWY. Thermal load and response monitoring of Ting Kau cable-stayed Bridge. In: Proceedings of International Conference on Innovation and Sustainable Development of Civil Engineering in the 21st Century, China Civil Engineering Society, Beijing; 2002. p.249–252.

[43] Lima JM, de Brito J. Inspection survey of 150 expansion joints in road bridges. Eng Struct 2009;31(5):1077–84.